ABSTRACT

Testing of New Front-End Electronics for the Hadron Calorimeter at CERN

John Lawrence

Director: Kenichi Hatakeyama, Ph.D.

The Hadron Calorimeter (HCAL), a major component of the Compact Muon Solenoid (CMS) detector at CERN, is designed to detect hadrons produced in proton-proton collisions supplied by the Large Hadron Collider (LHC). The HCAL is currently being upgraded with new readout modules that contain Silicon Photomultipliers (SiPMs), photodetectors that accept light from scintillator tiles and convert them to charge signals. Using a test beam capable of producing the same types of particles measured in the CMS detector, the new readout modules were tested in conditions like those of the CMS detector to fully understand their functionality before installation. Since the SiPMs in the new readout modules process the signals very differently from the hybrid photodiodes in the old readout modules, the analysis of test beam data provides insight into the features of the SiPMs. A virtual SiPM simulation was also created to assist in the analysis.

APPROVED BY DIRECTOR OF HONORS THESIS:

_____

Dr. Kenichi Hatakeyama, Department of Physics

APPROVED BY THE HONORS PROGRAM:

_____

Dr. Elizabeth Corey, Director

DATE: _____

TESTING OF NEW FRONT-END ELECTRONICS FOR THE HADRON

CALORIMETER AT CERN

A Thesis Submitted to the Faculty of

Baylor University

In Partial Fulfillment of the Requirements for the

Honors Program

By

John Lawrence

Waco, Texas

May 2018

TABLE OF CONTENTS

LIST OF FIGURES

ACKNOWLEDGMENTS

This thesis is the culmination of the research I did during my four years at Baylor University and has required hard work from many people. I would like to thank my thesis advisor, Dr. Kenichi Hatakeyama, for all of his continuous assistance, support in answering the numerous quesitons I had, and patience as I struggled through this project. I would like to thank Dr. Jay Dittmann, my work supervisor and the person who was always willing to carefully explain all the details I needed to know for my research. I would also like to thank all of the members of the Baylor High Energy Physics Research group as this research is very much a team effort.

CHAPTER ONE

Basic Particle Physics and CERN

Ever since ancient Greece, people have been trying to discover what makes up everything. Empedocles, an ancient Greek philosopher, said that everything was comprised of four elements: earth, fire, water, and air. Although modern scientists use more than four elements, they are still trying to categorize the most fundamental substance that makes up everything. Democritus proposed that everything, if divided enough times, could be broken down into atoms at their most fundamental level. While the term "atom" came to be known for something that was not the most fundamental substance, scientists today are still pursuing the "atom" theorized by Democritus.

In the 19th century, John Dalton believed he found the most fundamental particle and named it the atom, but as time passed, there was strong evidence that even atoms had internal components and structure. This was proven when J. J. Thompson in the late 19th century found the electron, which proved to be a component of the atom. The electron was not only the first fundamental particle discovered, but also the beginning of particle physics as a field of study. While it was an insightful discovery that led to many inventions, there were still many unknowns about the atom. About a decade after Thompson, Robert Millikan made fine measurements of the charge and mass of the electron, but this raised even more questions about the atom. In the early 20th century, Ernest Rutherford showed that the atom is mostly empty space with a very dense core called the nucleus, which has a charge opposite of that of the electron. In his experiment, Rutherford shot alpha particles, made up of two protons and two neutrons, at gold foil and observed their scattering angle. Most of the alpha particles passed through unperturbed, but a handful were significantly

deflected. From this observation, Rutherford concluded that most of the atom is empty space while having a highly dense core called the nucleus.

These discoveries showed that there were more things to explore beyond the atom. In parallel, there were equally important theories being developed. Quantum mechanics is essential to the study of subatomic particles, as they no longer behave according to classical mechanics. During this development, Max Planck was doing his work on the quantization of energy. This set the groundwork for quantum mechanics and also served as a basis to Einstein's work. Einstein formulated the important concept of light as a particle called the photon. Previously, light had been described as a wave, but Einstein showed that light had many particle-like properties including momentum. This theory and the more traditional view of light as a wave were combined, leading to the wave-particle duality of light. Eventually Louis de Broglie extended this duality to all particles, theorizing that all particles including electrons and other subatomic particles could be described using waves or particles.

Einstein's theory of relativity had another major impact on particle physics. The most famous of Einstein's equations, $E = mc^2$, shows the mass-energy relationship. One of the implications of quantum mechanics is that if something can happen it will happen under a certain probability. This means that given the right conditions and enough energy, one can create mass. There are other conservation laws, which need to be followed and are still relevant to particle physics, but conservation of energy is one of the biggest limiters. In order to create more massive particles, more energy is needed.

As these theories became more complete, they supplied a more complete picture of these subatomic particles, such as the electron states and the protons and neutrons in the nucleus of the atom. Scientists also began to find evidence of fundamental particles not in atoms. In 1932, Carl Anderson found evidence of a muon from cosmic rays. In addition, as scientists began to probe higher energies, they found

evidence of internal structure within protons and neutrons. In 1968 at the Standford Linear Accelerator Center, they found evidence of particles within protons, which were later called quarks.

The discovery of more and more fundamental particles led to the formulation of the standard model. The two main groups of particles in the standard model are fermions, which have half-integer spin, and bosons, which have integer spin. The main physical difference this causes comes from the Pauli exclusion principle, which allows fermions to combine into larger arrangements. Because of this, fermions are the building blocks of the macroscopic world as they make up protons, neutrons, and also atoms.

As shown in Table 1.1, there are several different groups of particles in the standard model. The first group is a subcategory of fermions called quarks. The main factor that distinguishes quarks from other fundamental fermions is that they interact via the strong force. While they also interact via the electromagnetic and weak forces, the strong force is the dominant one. Quarks can exist in isolation only for a short time and they quickly recombine in groups of two, three, or possibly more. When three quarks form a particle it is called a baryon. A proton, which is made up of two up quarks and one down quark, and a neutron, which is made up of two down quarks and one up quark, are both baryons. Each of the quarks inside a baryon has a different color — red, green, or blue — which serves as the "charge" for the strong force. Similar to electric charge, strong force color attracts other colors and repels similar colors, but since the baryon has one of each, it has a net color of white, or nothing. In addition to the six flavors of quark listed in Table 1.1, there is also a corresponding antiquark with the same properties but opposite charge and color. Quark and antiquark pairs can form color-neutral particles called mesons. If one tries to separate the individual quarks from the respective baryons or mesons, the energy required to separate them is more than the energy required to create more quarks.

For instance, when the constituent quarks in a proton are being pulled apart, there comes a point when the energy used to separate them is sufficient to create more quarks. This energy will be used to create new quarks leaving no quarks in isolation.

The other category of fermionic particles is leptons. Unlike the quarks, leptons are not affected by the strong force, and therefore it is more common to find them in isolation. The electron is the most well-known lepton, but there are also two other flavors that are heavier copies of the electron. As with all of the particles in the standard model, there are corresponding antiparticles for each lepton with the same mass, but opposite charge. In addition to the three charged leptons, there are also three neutral leptons, which are called neutrinos. Each one has a charged lepton partner. Neutrinos are nearly massless and do not have any charge. Since the only force that affects them is the weak force, they have a very low probability of interaction. This means that they essentially pass through everything without interaction. Although they do interact through processes such as beta decay, most neutrinos simply travel through everything.

Finally, there are the bosons. Bosons are different from both leptons and quarks in that they have integer spin, but the individual bosons differ from each other in which fundamental force affects them. While leptons and quarks combine together to form complex arrangements such as atoms and all of matter, bosons serve as the force carriers. The photon serves as the mediator for the electromagnetic force, which means that whenever two electrons repel each other there is a photon to mediate that interaction. The strong force interaction is mediated by the gluon. The weak force is mediated by the W boson, for those interactions with changes in charge, and the Z boson, for those interactions with no changes in charge.

One nice aspect of the standard model is that it gives this convenient table of fundamental particles, but the process of discovering all of these particles was not simple. The electron is the only particle in the standard model that is found in

Table 1.1. Particles in the Standard Model [4]

Particle Type	Name	Charge	Mass	Spin
Quarks	Up	$+2/3e$	$2.2\,\mathrm{MeV}/c^2$	$\pm 1/2$
	Down	$-1/3e$	$4.7\,\mathrm{MeV}/c^2$	$\pm 1/2$
	Charm	$+2/3e$	$1.28\,\mathrm{GeV}/c^2$	$\pm 1/2$
	Strange	$-1/3e$	$96\,\mathrm{MeV}/c^2$	$\pm 1/2$
	Top	$+2/3e$	$173.1\,\mathrm{GeV}/c^2$	$\pm 1/2$
	Bottom	$-1/3e$	$4.18\,\mathrm{GeV}/c^2$	$\pm 1/2$
Leptons	Electron	$-1e$	$0.511\,\mathrm{MeV}/c^2$	$\pm 1/2$
	Muon	$-1e$	$105.7\,\mathrm{MeV}/c^2$	$\pm 1/2$
	Tau	$-1e$	$1.776\,\mathrm{GeV}/c^2$	$\pm 1/2$
	Electron neutrino	0	≈ 0	$\pm 1/2$
	Muon neutrino	0	≈ 0	$\pm 1/2$
	Tau neutrino	0	≈ 0	$\pm 1/2$
Gauge Bosons	Photon	0	0	± 1
	Gluon	0	0	± 1
	W boson	$\pm 1e$	$80.4\,\mathrm{GeV}/c^2$	± 1
	Z boson	0	$91.19\,\mathrm{GeV}/c^2$	± 1
Scalar Boson	Higgs boson	0	$125.1\,\mathrm{GeV}/c^2$	0

isolation at energies common on earth. To find the next particle, the muon, scientists had to look at cosmic rays, which provided the energy needed to create these particles. While neutrinos are plentiful, they interact so infrequently that scientists are still struggling to create an efficient detector for them. To discover the remaining particles in the standard model, they had to use particle colliders. Throughout the last few decades, scientists have built colliders to probe higher and higher energies in order to make them capable of discovering more fundamental particles. In 2012, using the Large Hadron Collider at CERN, scientists were able to find evidence of the Higgs boson, the final particle in the standard model. Data showing evidence of the Higgs boson is shown in Figure 1.1. However, there are still phenomena in the universe that cannot be explained using the standard model, such as gravity and dark matter. There are several theories beyond the standard model that offer explanations for
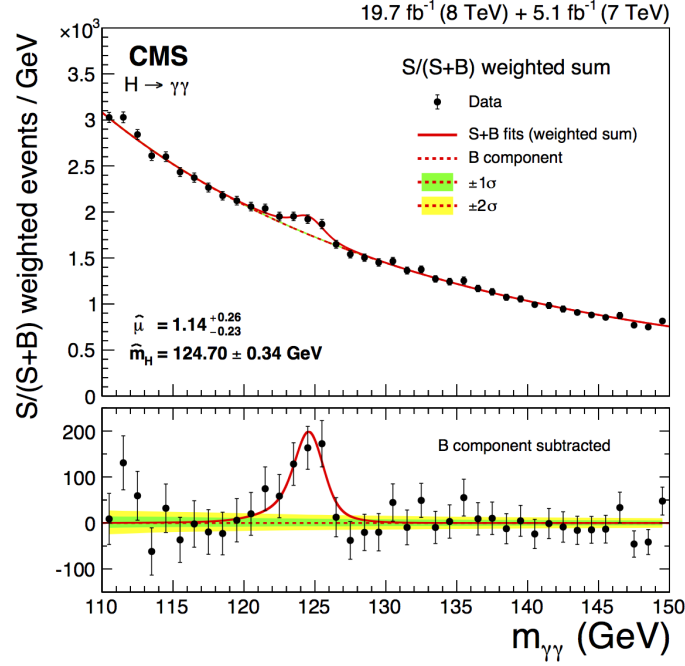
Figure 1.1. Two-photon invariant mass distribution from the CMS detector in 2012 [1]. The peak at $125\,\mathrm{GeV}/c^2$ is evidence of the Higgs boson.

these, but they also say there are more fundamental particles to be discovered at higher energies. This is one of the main goals of the LHC experiment.

After an upgrade that ended in 2015, the LHC is now capable of producing particle collisions at energies never before achieved. The LHC has also increased its rate of collisions. To be able to gather usable data from these higher energies and collision rates, the detectors on the LHC need to be upgraded as well. The Compact Muon Solenoid (CMS), one of the detectors on the LHC, is currently undergoing several upgrades. Chapter 2 will discuss the details of the LHC and the CMS detector. Chapters 3 and 4 will discuss the work I did for the CMS detector outlining the analysis done on new electronics that were installed in the detector during the winter of 2018 as a part of the upgrades.

CHAPTER TWO

Large Hadron Collider and Compact Muon Solenoid

2.1 The Large Hadron Collider

The LHC is located at CERN near Geneva, Switzerland. It has a circular shape and is 27 kilometers in circumference. It is about 100 meters underground, and as shown in Figure 2.1, it goes under the towns and farmland in the region. To look for undiscovered particles, the LHC collides protons at the highest energy ever achieved by a particle accelerator. After the most recent upgrade, the LHC now collides protons with a center of mass energy of 13 TeV, meaning the individual protons each have an energy of 6.5 TeV. The theory of special relativity says that a massive particle can only approach the speed of light but not attain it. As the protons in the LHC are traveling close to the speed of light it is more useful to use their energy rather than their speed. In addition, mass is often put into units of energy per speed of light squared, making the mass to energy conversion simple.

The process the LHC uses sounds simple when put into common terms. It accelerates protons to speeds very close to the speed of light and collides them at the center of a detector to see what comes out of these collisions. However, actually accomplishing this is not trivial. To start this process, electrons are stripped off from hydrogen gas, supplying the protons for the LHC. After this, the protons are put into a series of different accelerators, each designed to accelerate protons to higher and higher energies. The first accelerator is the Linac 2 linear accelerator, which pushes the protons up to 50 MeV. Then they are sent to the Proton Synchrotron Booster, which can push them to 1.4 GeV, after which the Proton Synchrotron ring accelerates the protons to 25 GeV. At this point protons are arranged into bunches such that a proton bunch passes by every 25 ns. This is the frequency at which protons collide

Figure 2.1. An aerial view of the LHC near Geneva, Switzerland [2].

in the LHC. Each bunch has about 100 billion protons in it. After sorted into these bunches, the protons are sent to the Super Proton Synchrotron where they achieve an energy of 450 GeV. Finally, the protons are fed into the LHC where they will be accelerated to their highest energy. An illustration of all of these accelerators is shown in Figure 2.2.

When the LHC has accelerated its particles to its peak energy, it collides them in the middle of four different detectors. LHCb, ALICE, ATLAS, and CMS [5] are the names of the four detectors that were built to study collisions supplied by the LHC. The CMS detector is the one I worked on during my undergraduate career, and is discussed in detail below.

2.2   The CMS Detector

The CMS detector is designed to detect particles coming out of the proton-proton collisions supplied by the LHC. As many different types of particles come out

Figure 2.2. The chain of accelerators that feed protons into the LHC.

of these collisions, the CMS detector consists of several different subdetectors, each designed to measure different properties of different types of particles. Going from the closest to the collision point outward, first is the Silicon Tracker. The Silicon Tracker is capable of finely measuring the path of the charged particles that go through it. The CMS detector produces a 4 Tesla magnetic field throughout most of the detector. As charged particles move through the magnetic field, their paths curve. The Silicon Tracker allows us to measure the curvature of their path and find their momentum. Next is the Electromagnetic Calorimeter, which is mainly responsible for measuring the energy of photons and electrons that come out of the collision. Then there is the Hadron Calorimeter (HCAL), which is responsible for detecting hadrons, which are particles made up of quarks, such as protons, neutrons, and charged pions. The HCAL, along with the other subdetectors, covers the collision point such that all paths out of the collision lead to the calorimeter. Since I did my work on the HCAL it is described in more detail in Section 2.2.1. Finally, there are the Muon Chambers.

9

Unlike other particles, the muon tends to go through the calorimeters only losing a small portion of its energy. This means the muons will reach the last section of the detector mostly unperturbed. Since the muons are charged, their path will be curved by the magnetic field so their momentum is measured by a process similar to that of the Silicon Tracker. An illustration of the different subdetectors and the particles that interact with them is shown in Figure 2.3.

Even with all of these subdetectors, there are still particles not directly detected. Neutrinos, for example, tend to go through everything without interacting, and they do not appear in our detector's signals. Several of the particles in Table 1.1 decay before ever reaching the detector. To find evidence of these particles we have to find indirect evidence of them. For example, the top quark decays nearly 100% of the time into a bottom quark and a W boson. The W boson then either decays into a charged lepton neutrino pair or a light quark antiquark pair. By finding evidence of these particles in close proximity, we can deduce that they came from a top quark.

2.2.1   Hadron Calorimeter

One of the main jobs of the calorimeter is to measure the energy of the incident particle. To accomplish this, an absorber, made with brass in the HCAL, is placed in alternating layers with scintillator tiles. When a particle hits nuclei in the absorber, it will produce a shower of secondary particles, which is called a hadronic shower. When these secondary particles hit the scintillator tile they will interact with the molecules in the tile, exciting them. These molecules will return to their original energy state emitting a photon. This photon, which is usually in the wavelength range of blue light, will travel through the tile into a wavelength shifting fiber around the edge of the tile, as shown in Figure 2.4. The fiber will "shift" the photon into a wavelength range of green light, keeping it from exiting the fiber. After traveling through the fiber the photon will enter a light mixer. This device will collect the light from multiple fibers, mix them, and send them to the photodetector, ensuring consistent and even
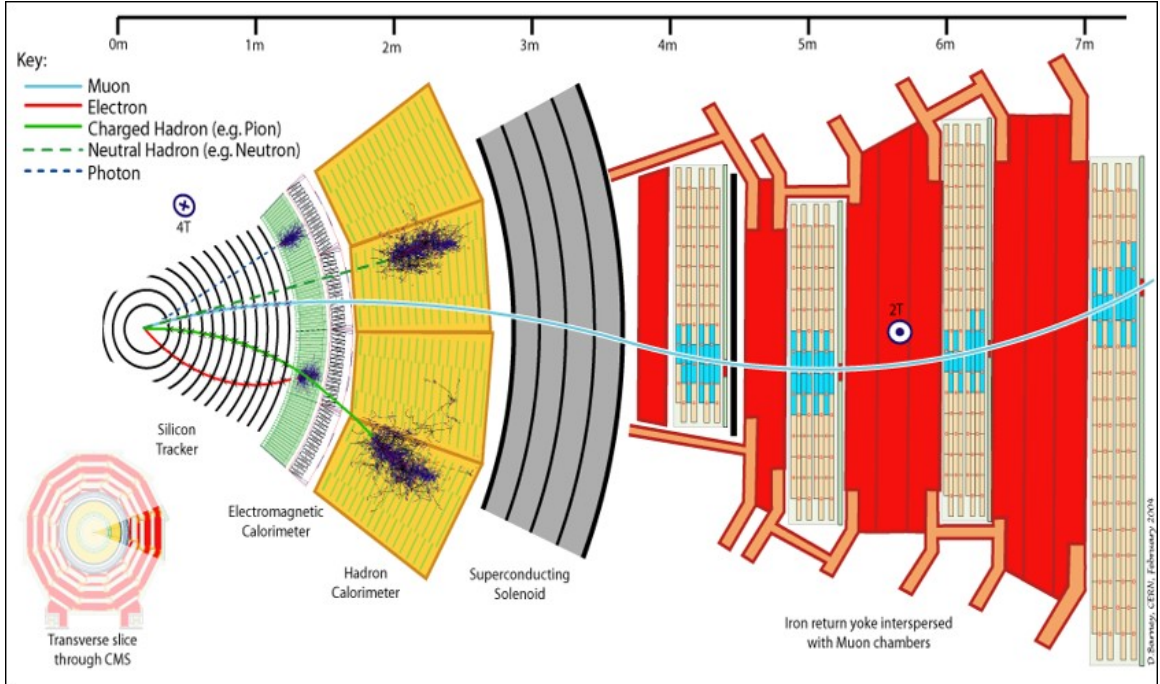
Figure 2.3. A slice of the CMS detector highlighting the different subdetectors and showing different particles and where they are stopped [3].

distribution of the light on the next component. The original photodetector for the HCAL was the hybrid photodiodes (HPD) [6] but they are being replaced by silicon photomultipliers as part of the upgrades to the CMS detector [7]. When the light is sent to the photodetector it will output charge proportional to the number of incident photons. The shower of secondary particles will scatter throughout several scintillator tiles, and summing the output charge over all of the tiles will give a measurement of the energy of the incident particle.

There are three main sections to the HCAL. Two of these are the Hadron Barrel (HB) [8], which surrounds the beamline like the edge of a cylinder, and the Hadron Endcap (HE), which caps off the cylinder made by HB. These two parts make a cylinder, which houses the beamline going through the center of the caps and the collision point in the center. Lastly there is the Hadron Forward (HF) section, which is in a shape similar to the HE but is located much further away from the collision
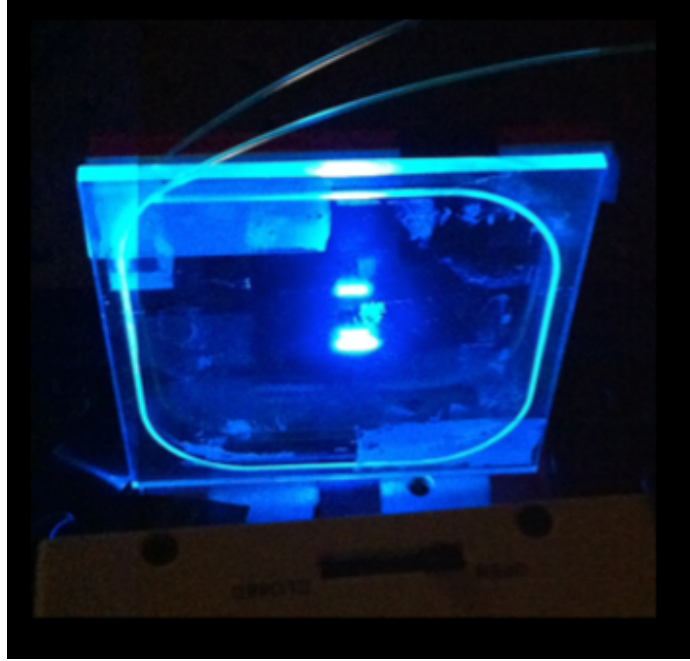
Figure 2.4. A scintillator tile with blue light and the wavelength shifting optical fiber around the edges and traveling out of the tile.

point [9]. To describe the geometry of the detector we use a coordinate system related to spherical coordinates with the origin being the collision point and polar angle of 0 being along the beamline. The azimuthal angle is denoted ϕ and the pseudorapidity angle η is related to the polar angle by $\eta = -\ln(\tan(\theta/2))$, which gives a value of 0 perpendicular to the beamline and $\pm\infty$ along the beamline. Usually these coordinates are arranged into discrete integer values denoted iphi and ieta, which are arranged such that a scintillator tile covers one ieta and one iphi as shown in Figure 2.5, but there are exception to this. For HB and HE there is also the segmentation in "depth" from the front face to the back end as shown in Figure 2.5, and each depth is denoted by an integer value.

2.2.2   Silicon Photomultipliers

The photons from the scintillator are sent to the SiPM, which has a circular array of small pixels. A picture of an array of SiPMs is in Figure 2.6. There are about
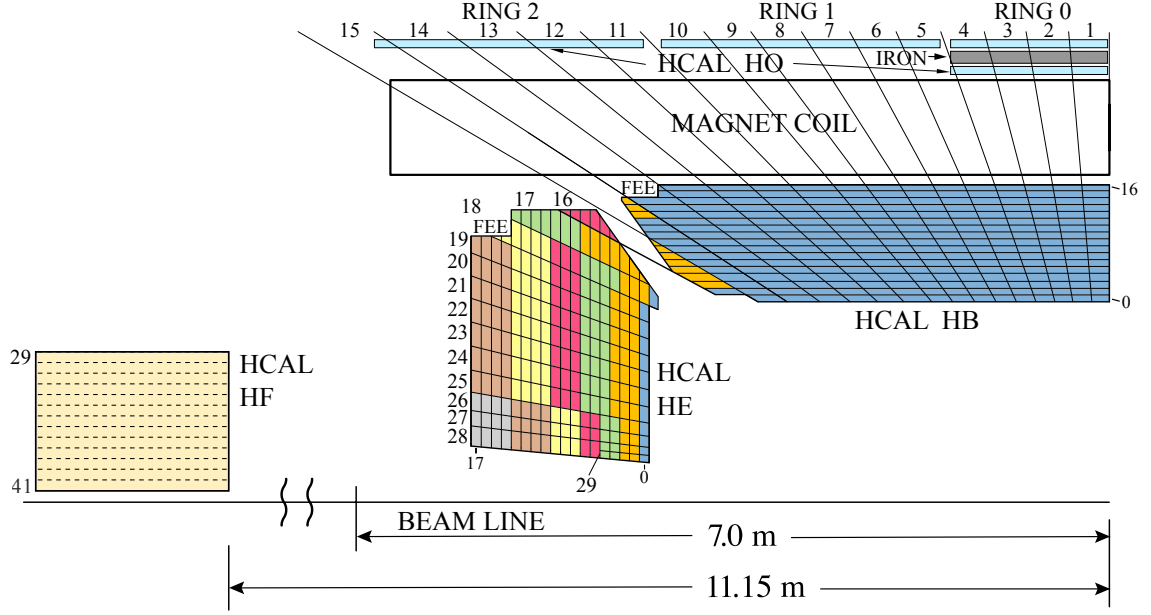
Figure 2.5. Layout of the HCAL showing a single iphi slice of HB, HE, and HF. Each box represents a scintillator tile for HB and HE. HF is read out by quartz fibers, and each channel that is read out by a bundle of quartz fibers is represented by a box.

33,000 pixels on a 3.3 mm diameter SiPM. When an individual photon hits one of the pixels on the SiPM it causes a capacitor to fire off a particular amount of charge. The total output charge of the SiPM is the sum of all of the pixels' output charge. Ideally, one just needs to sum the total amount of output charge of the SiPM and one can count the number of incident photons, since each pixel will fire off the same amount of charge. Counting the number of incident photons will give a measurement of the energy the particle deposited in the corresponding channel. There are some things that complicate the SiPMs readings. SiPMs are nonlinear devices, meaning the total output charge of the SiPM does not necessarily increase linearly with the number of incident photons. Experiments have shown the output charge per incident photon decreases as the total number of incident photons increases. At low incident photon count — on the order of 1,000 photons — the SiPM is very close to a linear device; however, as the incident number of photons increases the output charge does not increase at a steady rate. There are several factors that contribute to SiPM

13

nonlinearity, but the two main ones are cross talk and saturation. Cross talk is when a pixel is activated by a photon there is a chance that this activated pixel could activate some of its neighboring pixels artificially increase the output charge of the SiPM. When the photon hits a pixel it excites an electron causing an electron cascade and charge to flow. This excited electron has a chance to emit an IR photon, which could go in any direction. If it hits one of the neighboring pixels it could activate as if it were an incident photon.

Saturation occurs when a pixel is hit in rapid succession by multiple photons. When a pixel is hit by a photon it discharges its capacitor, which is the source of its output charge. After the pixel fires it needs some time (on the order of 10 nanoseconds) to recharge its capacitor. If the pixel is hit before it is recharged, it simply fires off whatever charge it has in its capacitor at the time, which could be reduced from its normal charge. Given that the SiPM has about 33,000 pixels when the number of incident photons is on the order of 1,000, the nonlinearity is insignificant, but particles can produce many more photons where this effect can be much more significant. The nonlinear properties of the SiPM makes it a bit harder to get accurate measurements, but there are ways to study them, which will allow us to compensate for these effects.
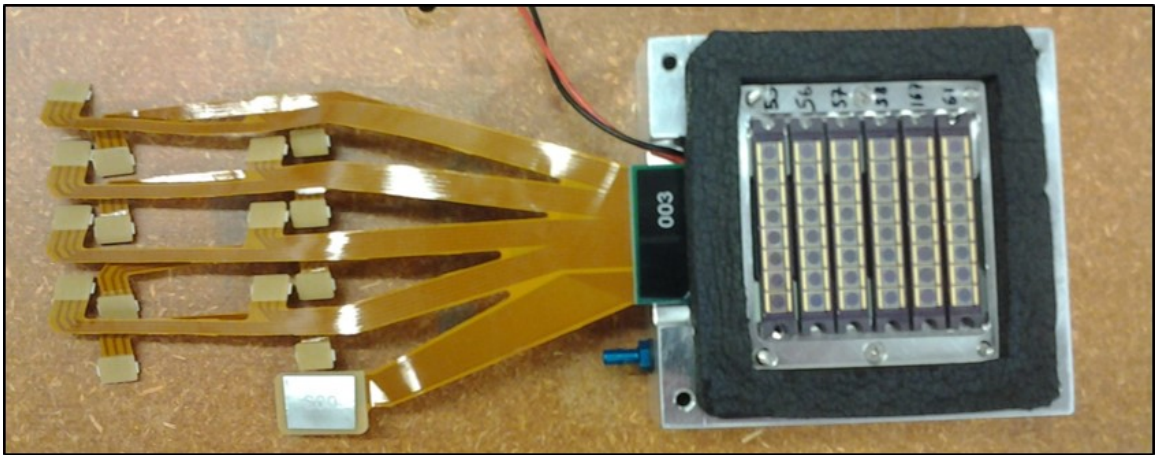
Figure 2.6. An array of silicon photomultipliers.

CHAPTER THREE

Test Beam

3.1 Test Beam Setup

The readout modules being installed in the CMS detector have several new components such as new charge integrator and encoder (QIE) chips [10, 11], but the main subject of my work was the SiPM. To study the features of the SiPM, such as nonlinearity, we used a test beam. The particles in the beam are at energies from about 10 to 500 GeV, and we can control the energy and types of the particles in the beam. There are several different experiments that use this beam, and the HCAL has a test stand that can be moved into the path of the beam when experiments need to be run. The CMS detector is 100 meters underground and is in a cavern that, due to radiation and tight enclosures, makes the detector difficult to access. Though modifications and maintenance can be made during shutdowns, this is not the ideal way to perform tests on new electronics. The test stand at the test beam location called H2 is on ground level and can be easily accessed. In addition, the energy and particle type of the beam can be easily controlled. The test stand is designed to be similar to a portion of the HCAL on CMS. Using this test beam, we can shoot particles such as pions at the test stand, which has the new readout module installed, and look at the response [12, 13]. We can vary the energy of incident particles, which should increase the number of photons produced in the scintillator tiles. This means there will be more input photons on the SiPMs.

We need to collect a large amount of data in order to measure the features of new readout modules with high statistical accuracy. To achieve this, we take multiple runs with several thousand events or particles hitting the test stand. Because we will be taking data over a long period of time, we want to ensure that we record data

only when a particle is hitting the test stand. One of the key systems that helps with this is the trigger system. In the path of the beam before the test stand we put scintillator tiles in order to send a generic signal to the control room. A total of four tiles were placed in the path of the beam. When we see signals from these tiles we know that a particle is coming from the beam. This serves as a trigger signal for our data acquisition system. The trigger signal then goes to the back-end electronics that stores the data from the detector. In this way we only store data around the time when we know a particle is hitting our test stand. There is also a ready signal that goes from the back-end electronics to the trigger. Since a particle may come before the back-end electronics are finished storing the relevant data, a trigger signal that comes without the ready signal will simply be ignored.

Although built to be similar to the HCAL on the CMS detector, the test stand is smaller and has some differences. When looking at the data from the test beam, it is important to be sure that the e-map, which traces the channels that receive the data to the actual scintillator tiles on the detector, is correct. There are some differences between the mock detector at H2 and the HCAL detector in the CMS cavern. In order to account for these differences, a new emap was created for the test beam setup. With an accurate e-map we can create an accurate picture of the incident particles hitting the test stand. The test beam allows us to control the energy and type of particles incident on the test stand. This allows us to study things such as SiPM nonlinearity as we can look at the output of the SiPMs under $50\,\mathrm{GeV}$ pions then increase the energy to $150\,\mathrm{GeV}$ and compare the different responses.

SiPM nonlinearity is not the only thing that is being researched using the test beam. In the test beam, the particles come at a low enough frequency, which allows us to isolate the signal of individual particles. This allows us to extract the pulse shape, which is the shape of the output charge vs. time. It is also important to see if the pulse shape changes significantly under different circumstances, for example, at higher

Figure 3.1. The HCAL test stand at H2. The scintillator tiles are covered in black tedlar and the new readout modules are connected in the back. The stand can be shifted so the beam can be aimed at different sections.

or lower energies. The well-measured pulse shape of individual signals is necessary information, since it is a vital input to the energy determination of individual incident particles in the CMS detector. Proton collisions occur every 25 ns under nominal LHC conditions; therefore, signals originating from subsequent proton collisions can overlap in time. The pulse shape information is used to resolve the overlapping signals in the CMS detector.

3.2 Test Beam Analysis

With a proper e-map, we can see its path and where it deposited its energy. Since a particle does not deposit all of its energy in a single scintillator tile, the e-map is critical when reconstructing the particle's energy from multiple neighboring channels. It is also important that there are often a variable amount of scintillator tiles in a single depth channel as shown in Figure 3.2, which shows four scintillator tiles in depth 5 and three scintillator tiles in depth 4. It explains why there is more energy deposited in depth 5 rather than depth 4.

Muons are useful for many things, but when trying to reconstruct the energy of particles, it is easier to use pions. The reason for this is that muons tend to go through the detector depositing a small portion of their energy and not being entirely stopped. This can be seen in Figure 3.2, which shows the muons depositing a nearly constant amount of energy in each of the depths, even the ones further along in the beam's path. Figure 3.3 shows that the majority of the events in this muon run produced several hundred fC in a single channel of the detector. Trying to reconstruct the energy of the incident muon would not give the actual energy, which would be significantly less than the actual energy of 150 GeV. On the other hand, Figure 3.4 shows a plot with a pion run. This shows that the pions deposit a large portion of their energy in the scintillator tiles of depth 2 and deposit less and less in the subsequent depths, with basically nothing in the last depth. There is also a more significant spread in energy compared to the signals in the muon run, which show the
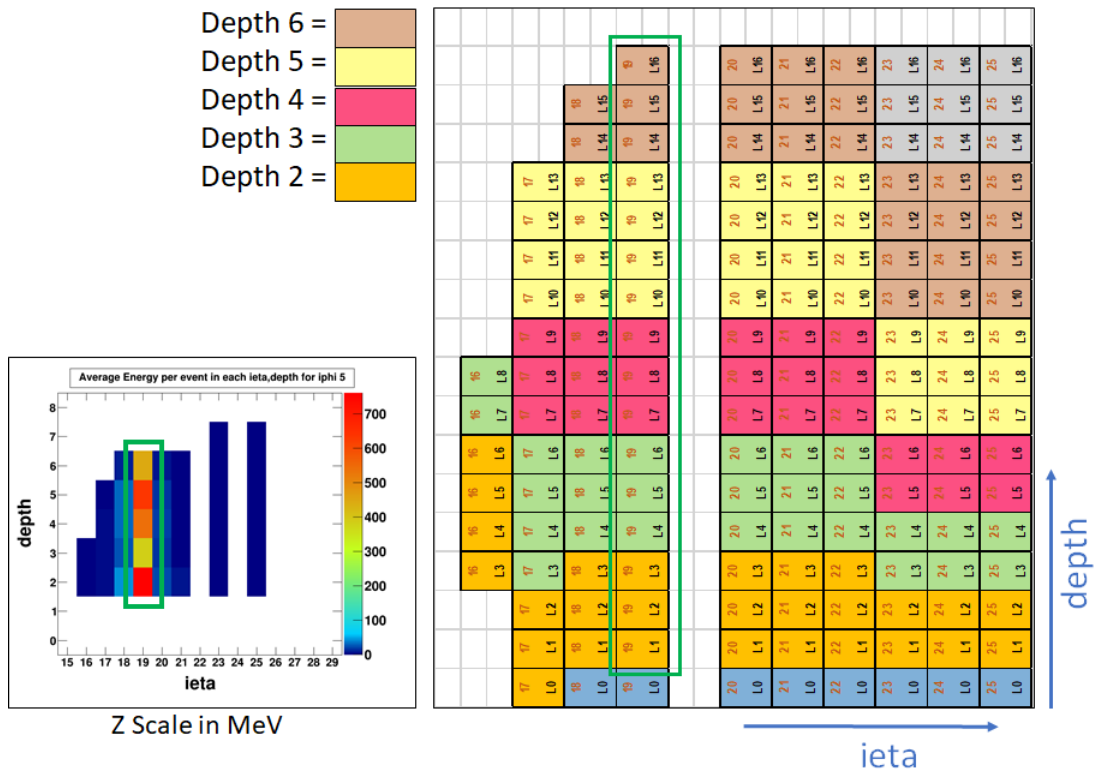
Figure 3.2. The emap for a iphi slice of the test stand on the right, which was used to create the figure on the left showing the different places the 150 GeV muons deposited energy in the test stand.
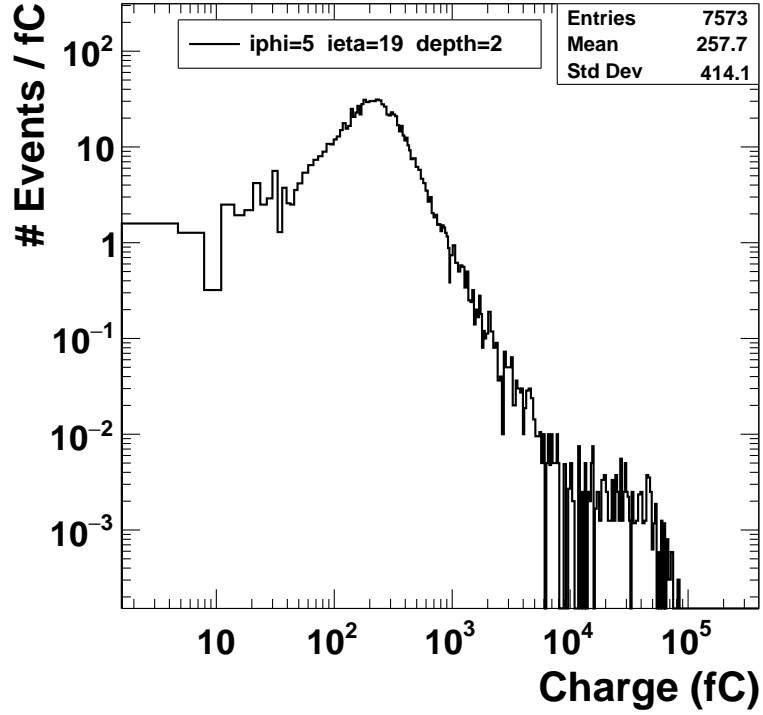
Figure 3.3. Charge distribution for a single channel (ieta 19, iphi 5, and depth 2) in a 150 GeV muon run. The beam in this run was aimed at ieta 19 and iphi 5.

muons going straight through while the pions leave some energy in the neighboring channels.

To reconstruct the energy of the incident particle we can look at plots such as those in Figure 3.5, which shows the mean output charge in a 50 GeV pion run. By looking at this output charge and the output charge of the other channels, we can find what portion of the particles' energy was deposited in this incident channel and then going by the known energy of the particle how much energy was deposited to produce this output charge.

The output charge distributions in events with different incident pion energies are shown in Figure 3.6, which shows the number of hits that output a certain charge. This figure can also be used to start the analysis on the SiPM nonlinearity. One key
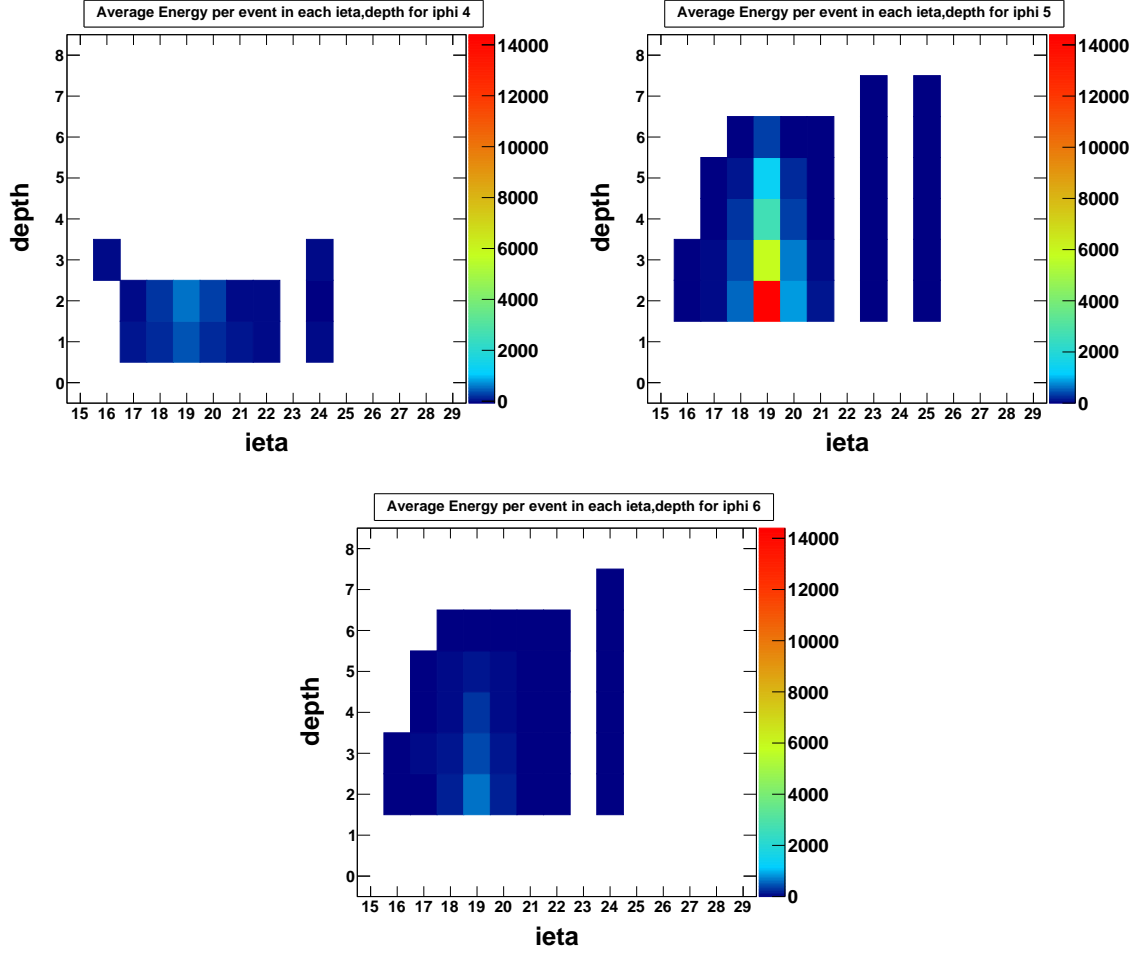
Figure 3.4. Average energy deposited (in MeV) in the channels in the test beam during a 50 GeV pion run aimed at ieta 19 and iphi 5. The different plots show the different iphi locations.
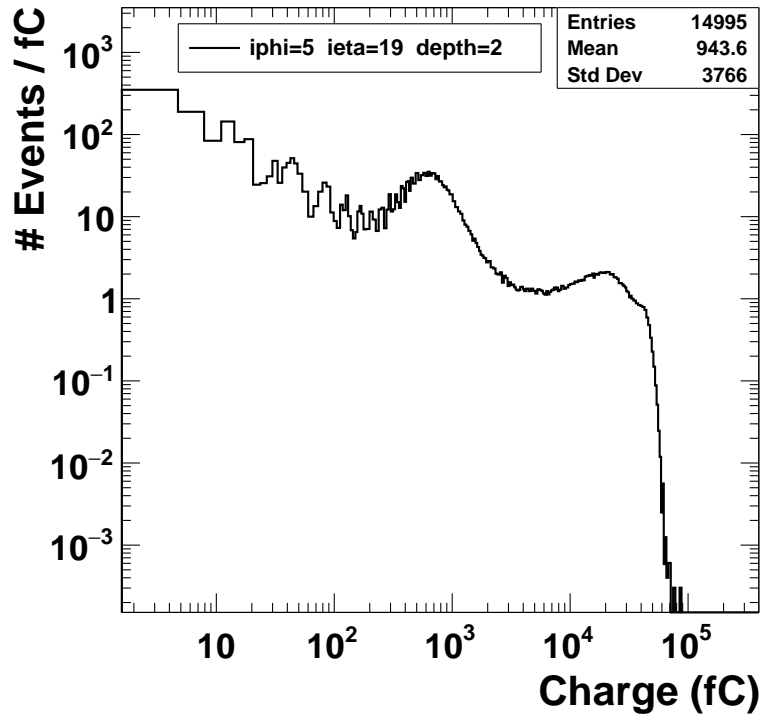
Figure 3.5. Charge distribution for a single channel (ieta 19, iphi 5, and depth 2) in a 50 GeV pion run aimed at ieta 19 and iphi 5. The peak on the right shows the average output charge in response to the incident particles at this energy.

thing about the nonlinearity is that at low charge output and correspondingly low particle energy, the SiPM is expected to have a linear output, and only at high output charge does this effect become significant. This means that, in order to study nonlinearity, one needs to use particles at sufficiently high energies. Unfortunately the highest beam energy that can be achieved with the test beam yields a signal in the range in which the SiPM nonlinearity effect is only at a few percent. To illustrate this, by looking at Figure 3.6 it is apparent that in the 300 GeV run, an energy close to the maximum the test beam is capable of producing, there are minimally few events that output charge above 300,000 fC. The SiPM outputs approximately 40 fC for every incident photo electron, which means the highest energy events create about 6000 incident photo electrons. When using a simulation of the SiPM it is apparent that this is still very much in the linear range of the SiPM. One thing to note is that not all of a single particle's signal goes to a single SiPM. Figure 3.5 shows that while the majority of the particle's energy is deposited in the first group of scintillator tiles it hits, there is still a significant portion in neighboring channels. Summing over all the channels should give the total energy of the particle, but this means that 300,000 fC does not directly translate to 300 GeV. As the energy of the particle increases its energy will spread out more, which means a 600 GeV pion will not necessarily deposit 12,000 photo electrons in the first channel it hits.

One of the key things in doing a pulse shape analysis using test beam data is the timing information. In the test beam, we have two different pieces of timing information. The first comes from the QIE chips in the readout modules. The readout modules measure the output charge of the SiPM over 250 ns, and the information is binned into 10 time samples each 25 ns long, which is shown in Figure 3.7. The output pulse of the SiPM is about 75 ns long, and it usually stays confined to 3 or 4 time samples. In addition, we also record what is called a Time to Digital Converter (TDC) value. This value stores at what time in the 250 ns span the output charge of

Log Charge Distributions

30 GeV Pion
80 GeV Pion
100 GeV Pion
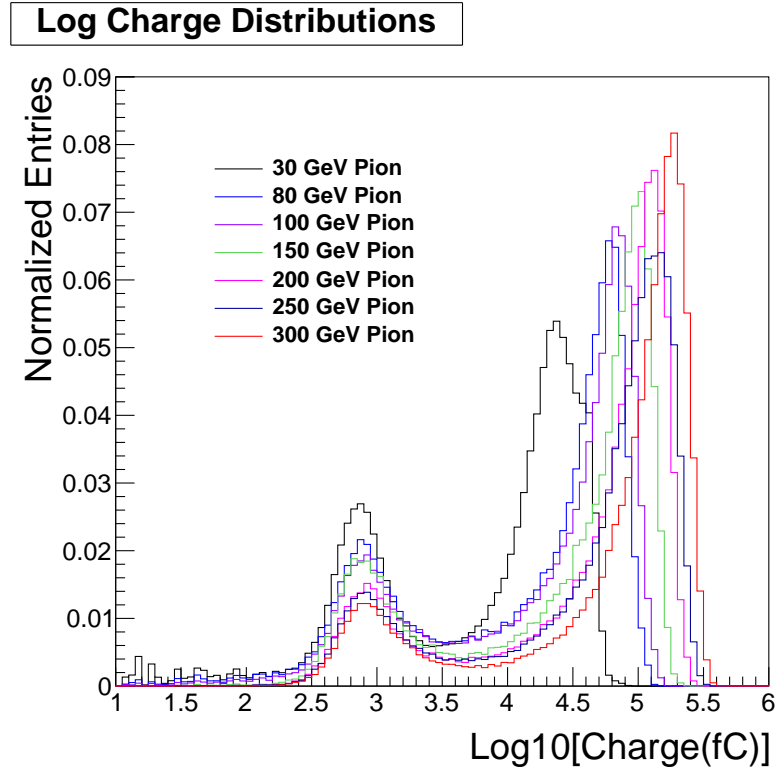150 GeV Pion
200 GeV Pion
250 GeV Pion
300 GeV Pion

Figure 3.6. Distributions of charge signals from the channel iphi 5, ieta 19, and depth 2 in events with different pion energies.
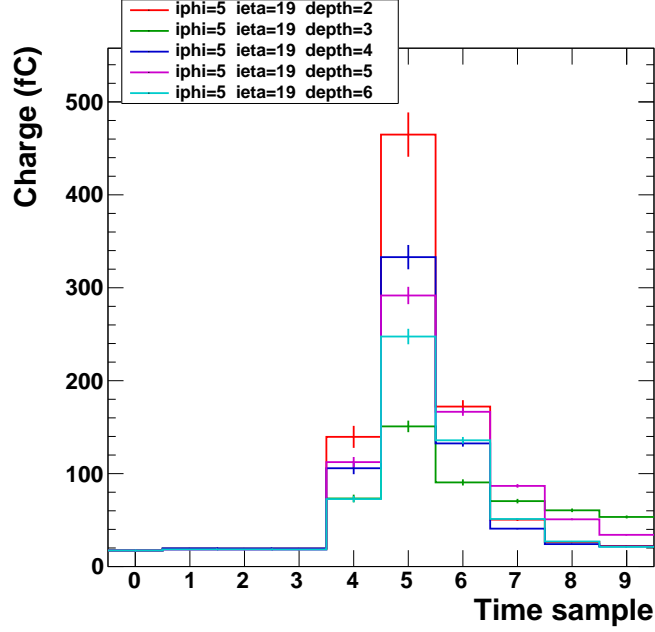
Figure 3.7. The average output charge over time in ten time samples, each 25 ns long. This is from a run with 150 GeV muons aimed at iphi 5 and ieta 19. This plot shows the output pulse of the different depths at that location.

the SiPM crossed a threshold, with 0.5 ns resolution. Since the output charge starts out below this threshold, the TDC value should give the start of the output pulse of the SiPM. For instance, a TDC value of 20 in time sample 4 means that the pulse crossed the threshold charge value 10 ns after the start of time sample 4 or 110 ns after the start of data taking. One of the problems with the TDC value is that it could be affected by the amplitude of the output pulse as a high amplitude pulse will cross this threshold earlier. To extract the pulse shape we can take the difference of pulses with different TDC values.

There is also timing information from the trigger system. The timing information from the trigger system does not have the amplitude dependence, which the TDC timing information may have; however, most people still use the TDC from the
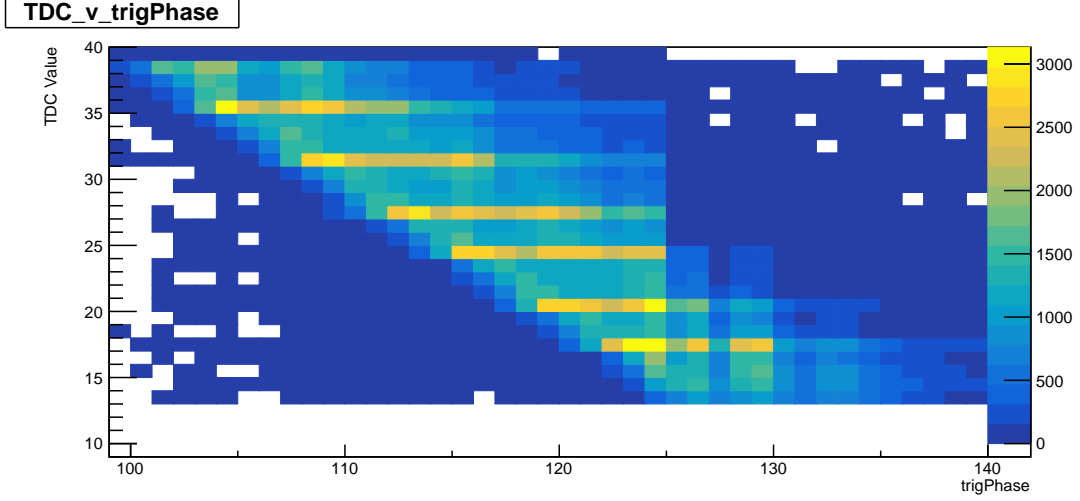
TDC_v_trigPhase

Figure 3.8. The correlation between the trigger timing information and the QIE TDC information.

QIE chips. The relationship between the two signals can be shown in Figure 3.8. Theoretically, this timing information from the trigger system could be used to extract the pulse shape.

When we take a run using the test beam, we do not just take data from one single particle but several thousand stored in their own individual events. Because of the nature of the test beam, there is some randomness in the arrival time of the particles in the beam. When extracting the pulse shape, we use this randomness by looking at pulses with the same total charge but different TDC values. Theoretically, two pulses with the same charge but different TDC values should be exactly the same except for a time shift. These pulses could look different in data, however, as different parts of the pulse will be put into different time samples. Figure 3.9 shows an analog pulse shape along with its binned output. In our analysis method, to extract the pulse shape, we take the difference in binned pulse value from several different pulses, all with similar overall charge but with a range of TDC values. Figure 3.10 shows multiple sets of data, all with different TDC values, illustrating how changing the TDC value can change the bins without changing the total output charge. An
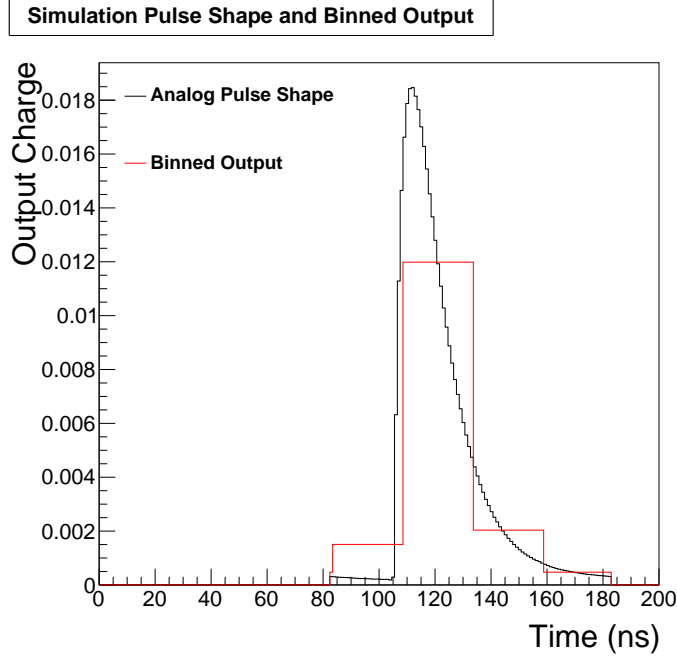
Figure 3.9. A SiPM simulation showing an analog version of the output charge along with the same output binned into time samples of 25 ns.

example of this is taking the difference in the charge value from time sample 4 in a pulse with a TDC value of 20 and the charge value from time sample 4 in a pulse with a TDC value of 21 gives the pulse height at 110 ns in the 250 ns long data set. Doing this process over all the time samples with more pulses and TDC values ranging from 0–49 in time sample 4 will give a more analog version of the pulse shape shown in Figure 3.11.

When we extract the pulse shape from test beam data, we use events that have similar output charge. There are a variety of reasons for this, but one of them is that there is evidence that the pulse shape changes with output charge. To study this, we measure the pulse shape using events with different output charge and see if there are any significant changes. Although most of the particles will have an energy identical to the beam energy, it is common to have outliers. To minimize this disturbance we take events from several different runs with particle energies ranging all the way from 30 GeV to 300 GeV and collect together the events in which the output charge
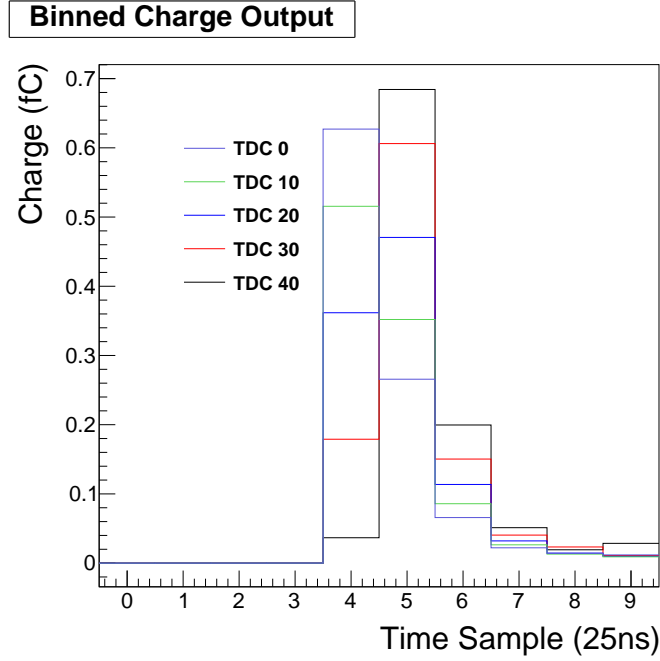
28

Binned Charge Output

Figure 3.10. The binned output charge of events with different TDC values. All pulses have their TDC value in time sample 4 and have a total output charge in the range of 50,000–80,000 fC.
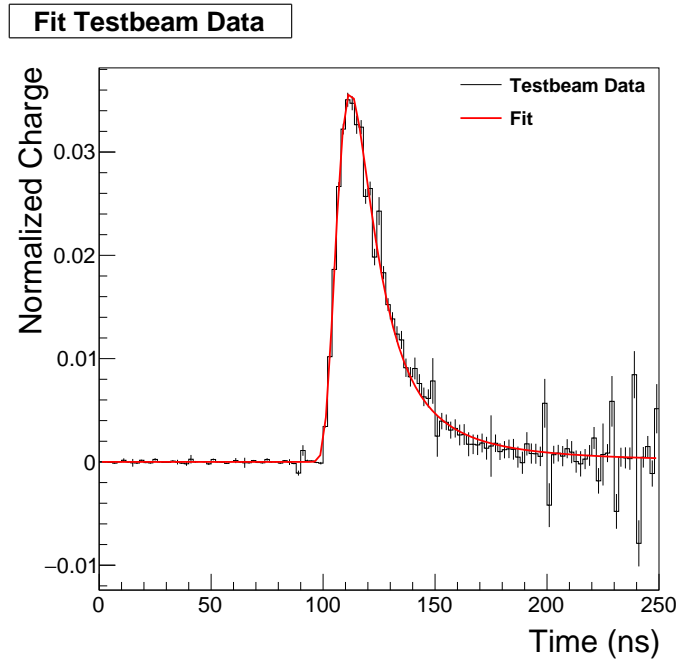

Fit Testbeam Data

Figure 3.11. A more analog version of the SiPM pulse shape obtained from test beam data. It is also fit to a Landau-Gaussian function. The total output charge of signals used to extract this pulse shapes ranges from 10,000 to 29,000 fC.

falls in a certain charge range. Figure 3.12 shows pulse shapes obtained from several different charge ranges. Figure 3.13 shows the fits of these pulse shapes superimposed for comparison purposes. These fits show that there is little change in the pulse shape as the charge increases, but there is a small trend visible in this plot. Looking at the peak of the pulses it is apparent that the lower charge pulses have lower peak heights. This lack of area is made up in the second half of the pulse as the lower charge pulses are slightly higher there, though this is harder to see as it is over a longer period of time. This result is not unexpected as the nonlinearity of the SiPM can shift the charge of the pulse towards the front.

3.3 Summary

Using test beam data, we were able to extract a precise pulse shape of the new readout modules. This pulse shape does appear close to expectations and has a reasonable fit to the Landau-Gaussian function. The pulse shape does show minor changes with changes as the output increases but at the energies from the test beam this effects was negligible. The nonlinearity of the SiPM was not able to be studied in depth using the test beam data, but we were able to confirm that at energies from the test beam the SiPMs are very close to linear. These readout modules were installed in the HE on the CMS detector over the winter of 2018.
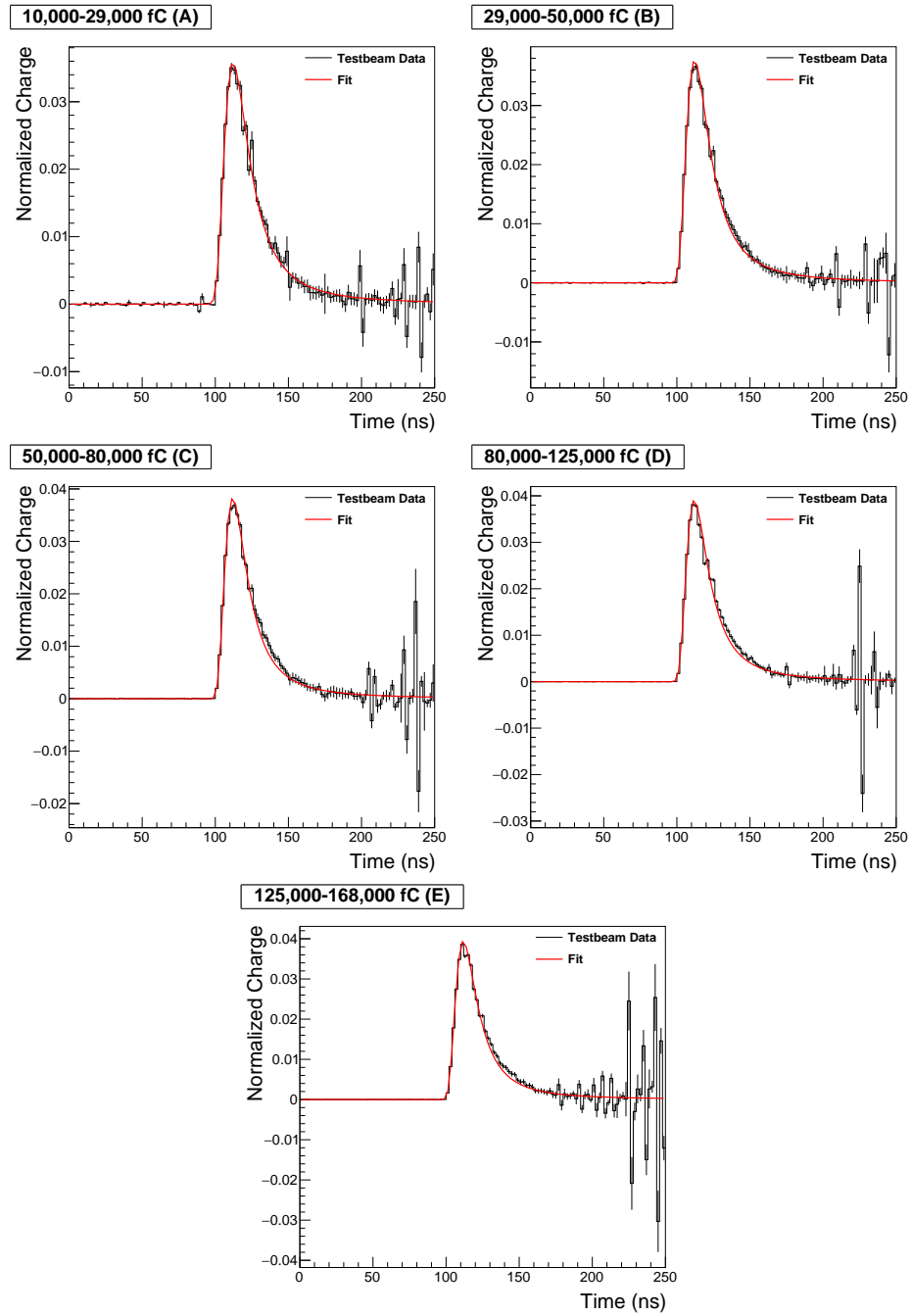
Figure 3.12. Fitted pulse shapes for signals in the charge range (A) 10,000–29,000 fC, (B) 29,000–50,000 fC, (C) 50,000–80,000 fC, (D) 80,000–125,000 fC, and (E) 125,000–168,000 fC.
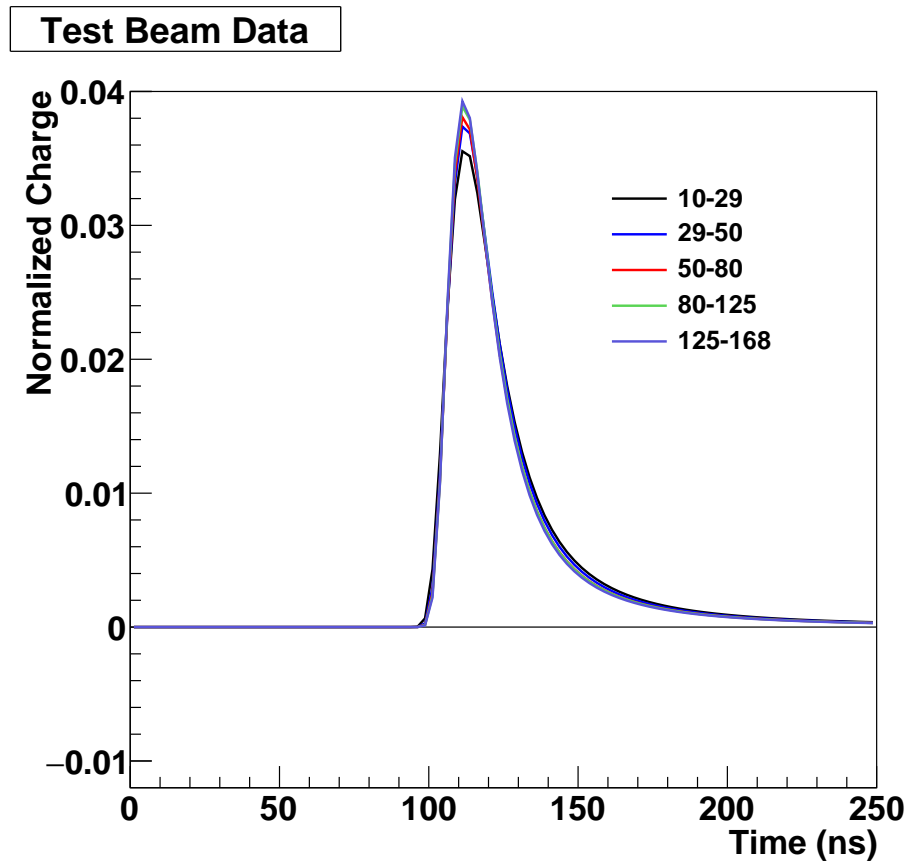
Figure 3.13. Comparison of fits to pulse shapes obtained from different charge ranges.

CHAPTER FOUR

SiPM Simulation

4.1 SiPM Simulation

In addition to studying the new electronics with the test beam, we also created a SiPM simulation that takes theoretical input signals from the detector and calculates the SiPM's response [14]. When light from the detector goes to the SiPM, a light mixer is used so that the light is spread across the pixels on the SiPM. The intensity of light on the SiPM over time is described by the so-called Y11 pulse shape, because its shape is mainly due to the Y11 wavelength-shifting fiber that takes the photons from the scintillator to the SiPMs. The Y11 pulse shape is shown in Figure 4.1. Using a mathematical representation of this pulse shape, we can simulate how light is shined on the SiPM. We can then create a virtual SiPM that has an accurate geometric representation of the pixels. Each of these virtual pixels could be activated by the incoming Y11 light pulse and would respond by firing off a set amount of charge like an actual SiPM. When these pixels are activated, they also have a certain probability to activate neighboring pixels, which simulates the cross talk of the SiPM. Each pixel also has a recharge rate such that, if hit in rapid succession, it will fire with a reduced amount of charge, which emulates the saturation effect. In this simulation we can easily adjust the number of input photons and obtain details of the SiPM response. We can also turn on and off different features of the SiPM in order to see how significant individual effects are. Using the simulation, it is simple to change the type of input to a precise situation and gather large quantities of data. The accuracy of this simulation is heavily dependent on the data we input into it.

Since the program can simulate the nonlinearity effects of the SiPM, we can use theoretical inputs to the SiPM to study its effects. As the Y11 pulse shape does not
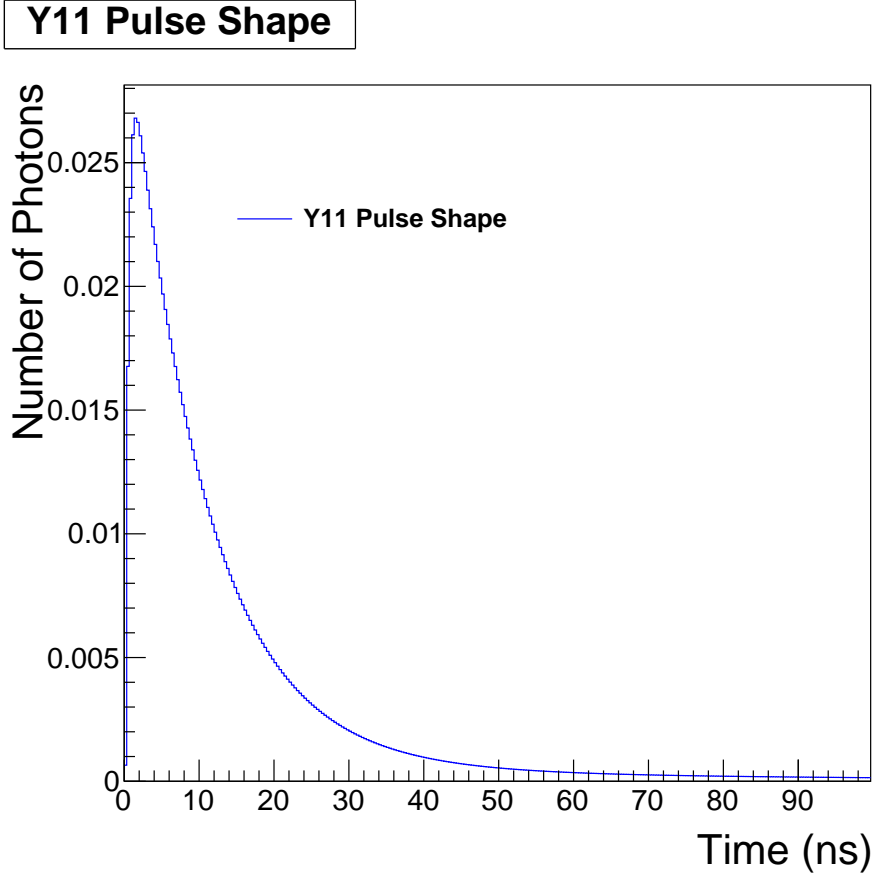
Figure 4.1. The Y11 pulse shape used in the SiPM simulation.

change with the number of photons or other situations, to simulate a higher energy particle, we simply need to increase the total number of photons in the incident pulse. The output of the virtual SiPM is normalized so that if the SiPM were a completely linear device, its output "charge" should exactly equal the number of input photons.

4.2 Simulation Analysis

To do the analysis using the SiPM simulation, we simply measure the total output of the SiPM over a light pulse and compare it to the number of input photons. Since there is a degree of randomness, we will use the average pulse over several inputs. Compared to using test beam data, the analysis with the simulation is simple. In the test beam, the energy of the particle is spread over several SiPMs, while in the
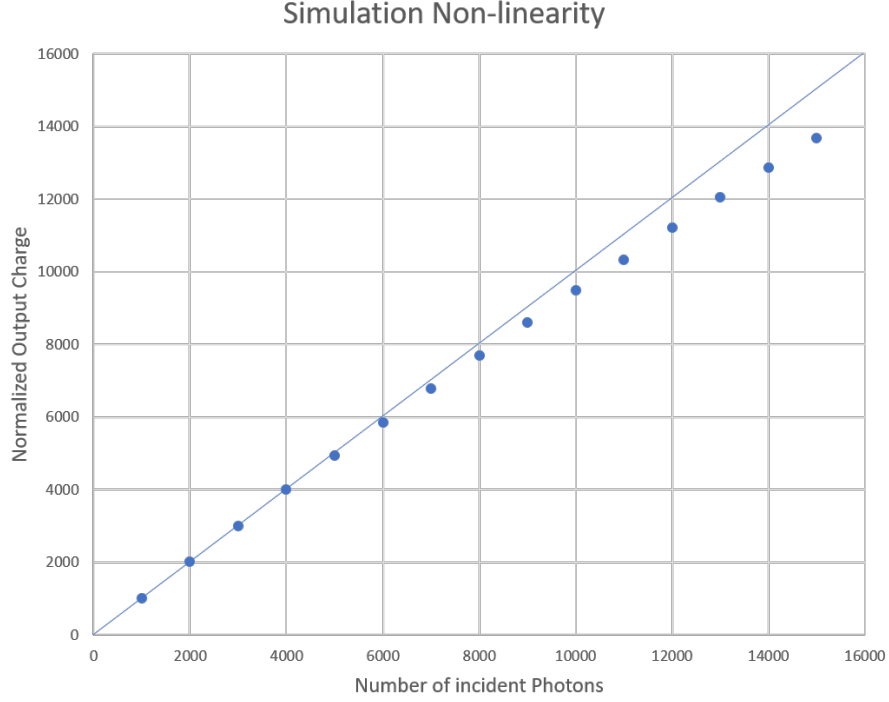
Figure 4.2. The number of incident photons vs. output charge of the SiPM simulation with a $y = x$ line for reference. Given the units of the simulation, a perfectly linear device would have all data points falling on the $y = x$ line, but as shown, as the number of incident photons is increased the data points fall short of this line.

simulation we have very fine control of the input energy to the single SiPM. With a plot of input number of photons vs. SiPM output charge, we then create a correction curve that is necessary to make the graph linear. This is a process for doing a nonlinearity analysis using test beam data so that we can compare the two correction curves to see if there is agreement. With other analyses it is common to simply divide out the cross talk. Given that there is a 15.4% chance of crosstalk with a large signal of several thousand photons, it is assumed that 15.4% of the signal from the SiPM is due to cross talk, so that charge is ignored. This means the majority of the effects that the correction curve is compensating for is saturation. Figure 4.2 shows the nonlinearity obtained from the simulation.
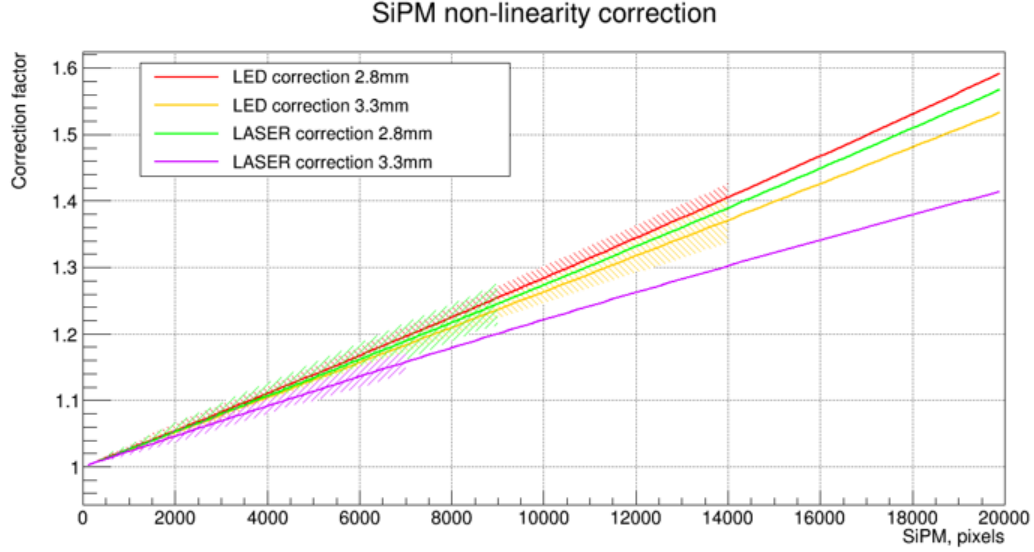
Figure 4.3. The SiPM nonlinearity correction factor vs. number of pixels fired. The correction factor is the number the output needs to be multiplied by in order to obtain the linear output value. This means a perfectly linear device would always have a correction factor of 1. This data was obtained by shining a laser directly on the SiPM.

To be sure the simulation is designed correctly, it is useful to compare things such as nonlinearity to the actual SiPM. Figure 4.3 shows the nonlinearity of the SiPM from shining a laser directly on the SiPM. Figure 4.4 shows a similar plot constructed using the simulation. There is significant disagreement between these two sets of data.

One effect of saturation that is less understood and harder to implement is that the pixels can sometimes recharge faster. This effect is due to the QIE chips in the readout modules which, in addition to taking and processing the charge from the SiPMs, also supply the charge that recharges the capacitors for each individual pixel. The capacitors for the pixels recharge exponentially, as expected from normal RC circuits. Normally the time constant for the capacitors is about 9 ns, which means the capacitor is completely recharged after 20 ns, but this is when the SiPM is outputting a very low amount of charge to the QIE chips. When the SiPM is outputting more charge, the QIE chips supply more charge to the SiPM, recharging the pixels faster.
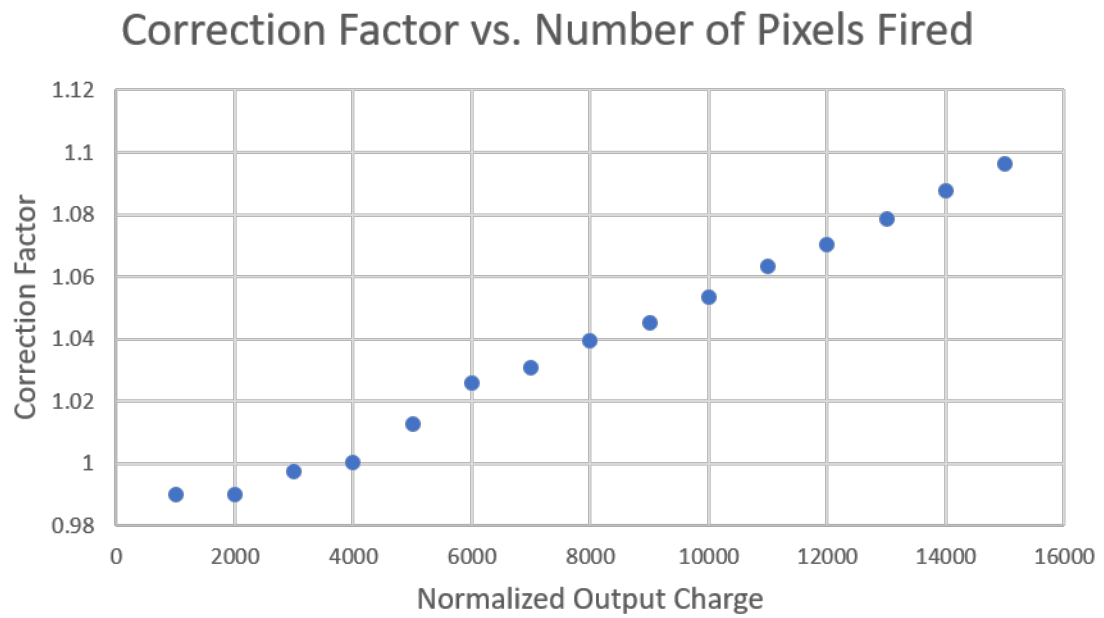
Figure 4.4. The correction factor vs. number of pixels fired. The correction factor is the value that the output needs to be multiplied by in order to obtain a linear output value. This means a perfectly linear device would always have a correction factor of 1. These data was obtained from the SiPM simulation.
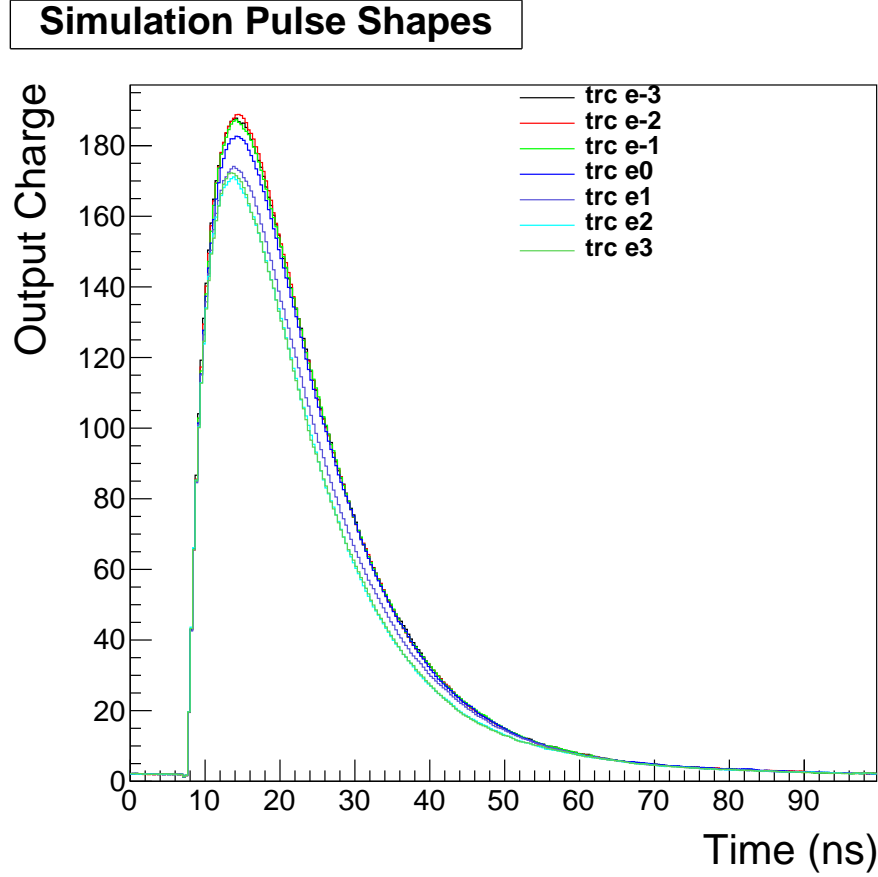
Figure 4.5. Output pulses of the SiPM simulation with 1,000 incident photons comparing the effect of changing the recharge time constant on the pixels. The TRC value is the recharge time constant ranging from 10^{-3} to 10^{3}.

When the pixels recharge fast, they fire off charge closer to the maximum charge even when hit in rapid succession. This means the effects of saturation are diminished when the output charge of the SiPM increases. The effect of different recharge time constants for the pixels can be seen in Figure 4.5.

Using the simulation we can also look at the pulse shape of the SiPM. This pulse shape should theoretically be the same as that obtained from test beam data. One of the main things that is interesting to look at is "does the pulse shape change significantly with a change in input energy?" As shown is Figure 4.6, the output pulse shape does not significantly change with different energies.
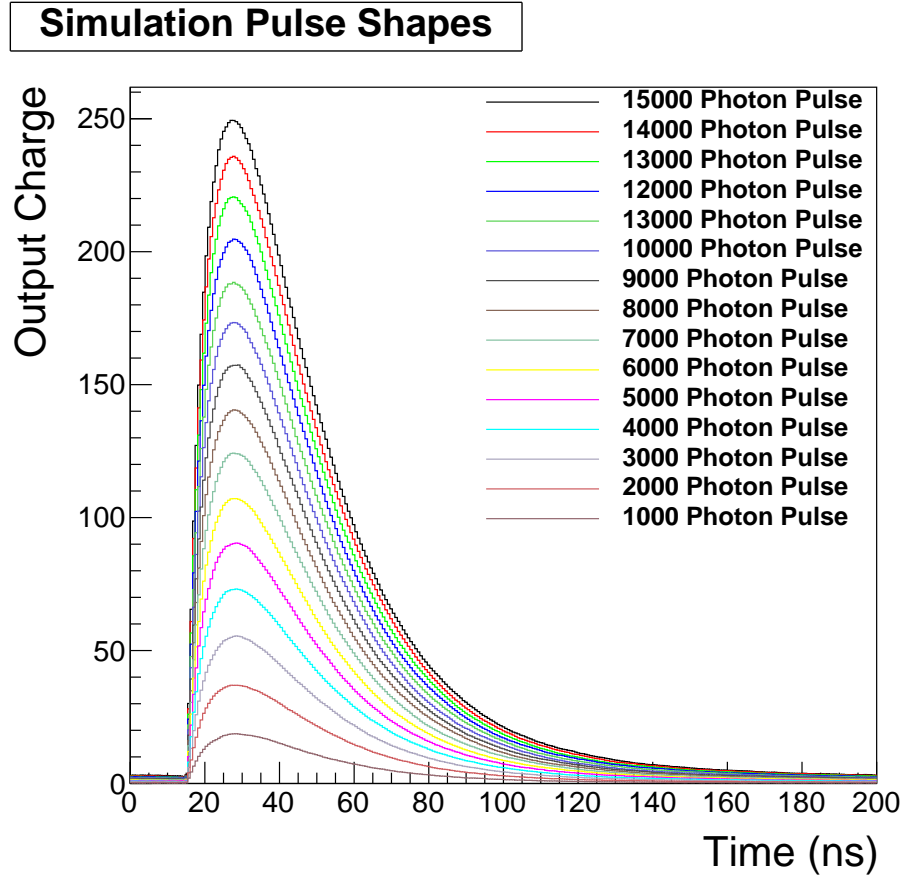
Figure 4.6. Pulse shapes from the SiPM simulation. They are overlaid on top of each other to highlight any differences from increasing the input photon count.
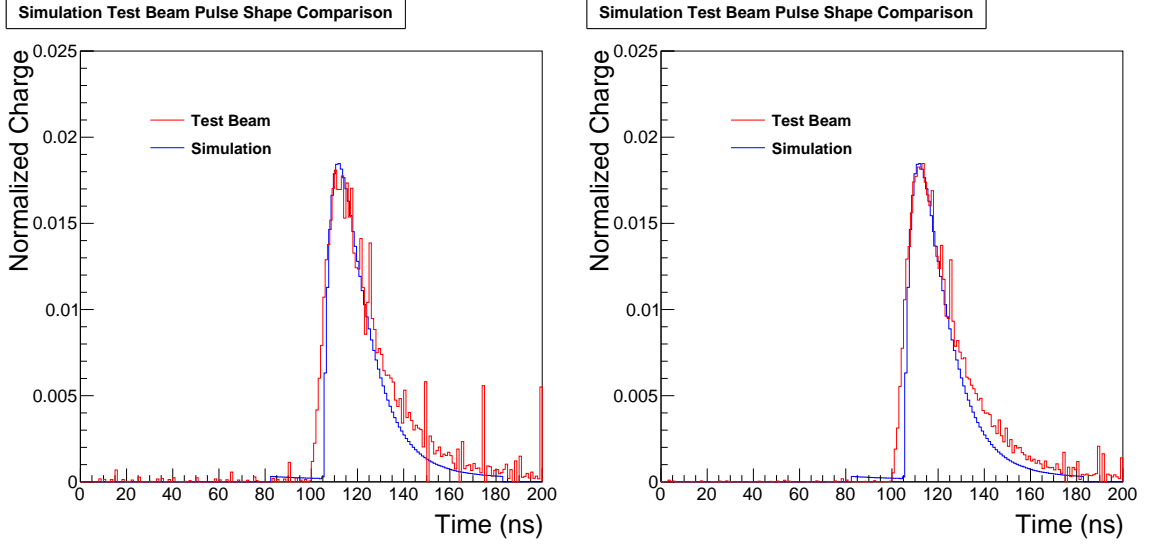
Figure 4.7. The pulse shapes from the simulation and the test beam data, overlaid for comparison purposes. On the left the charge range is 10,000–29,000 fC and on the right it is 29,000–50,000 fC.

We can compare the pulse shape from the simulation to the one obtained from test beam data. These pulses are expected to be the same. For comparison we simply plot the two pulse shapes on top of each other and see if there are any major differences. To minimize the interference of other effects such as nonlinearity, we can compare pulses from similar output charge. Using the conversion ratio of 40 fC to 1 photon, we can compare pulses from the same charge range. We compare the pulse shape from the charge range 10,000–29,000 fC to one from the simulation results from 500 input photons. Figures 4.7 and 4.8 show these comparisons. While they do have the same basic shape, there are some differences — mostly, the simulation is much narrower in the base.

4.3   Summary

The simulation is a useful illustration for how the SiPM works, and it can be easily adjusted for future modifications. Some of the plots used in this thesis to explain how a SiPM works were created using this simulation. The analysis of the
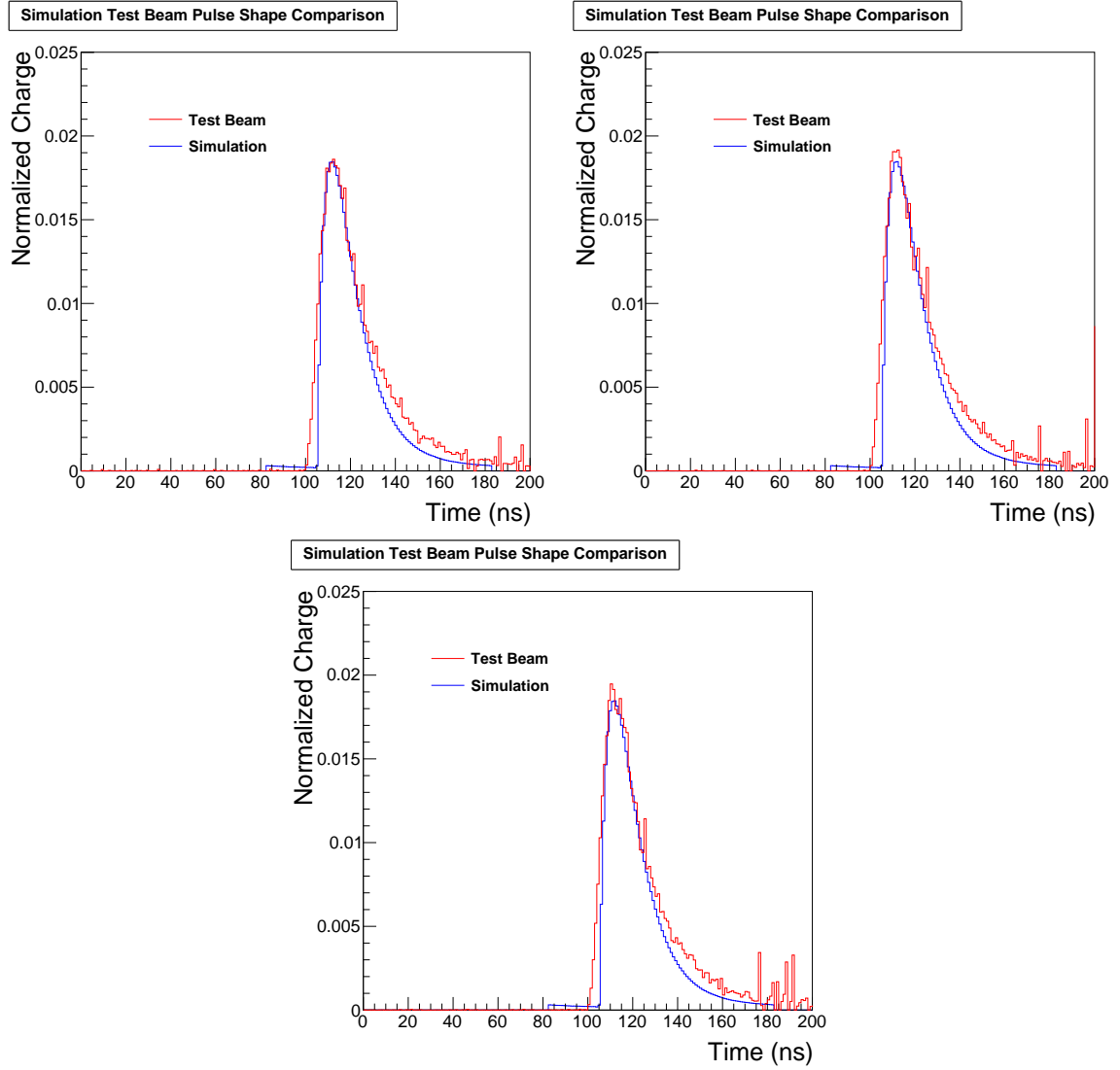
Figure 4.8. The pulse shapes from the simulation and the test beam data overlaid for comparison purposes. On the left the charge range is 50,000–80,000 fC, on the right it is 80,000–125,000 fC, and on the bottom it is 125,000–168,000 fC.

simulation, however, shows that there are still some major flaws with the simulation. The pulse shape comparison shows that the simulation shape is narrower in the base than the measured pulse shape. In addition, the nonlinearity in the simulation is much smaller than measurements made using an actual SiPM. The reasons for these discrepancies are still being investigated, but there are several leads. Among them are the changing recharge times and other effects such as the scintillator tiles and QIE chips not yet taken into account in the simulation.

CHAPTER FIVE

Conclusions

The CMS experiment at the LHC has had many successes, including the discovery of the Higgs Boson in 2012. In order to search for undiscovered particles, the LHC was upgraded to be able to produce collisions at higher energies and at a higher rate. The CMS detector also had to undergo an upgrade in order to benefit fully from the upgraded LHC. I worked on the testing of new readout modules for this upgrade in the CMS detector. The readout modules performed as expected in the tests and showed they were capable of performing the task for which they were designed.

In this thesis, I presented my analysis on the new readout modules, with a focus on SiPM features and pulse shape extraction. The pulse shape analysis using the test beam data was very successful. It was expected that the pulse shape would be similar to a Landau Gaussian function, which is what the analysis showed. The signal pulse shape was also found to be approximately the same over different charge ranges. This pulse shape will allow the extraction of individual particle signals in the CMS detector.

The non-lienarity of the SiPM was another feature I studied, but it could not be analyzed in depth due to limitation of the signal amplitudes from the test beam. The SiPM is approximately linear at low incident photons. To study the SiPM nonlinearity, a particle at an energy that will produce a number of photons in the nonlinear range is needed, but the test beam was not capable of producing particles at the needed energies. The test beam did show an energy range for which the SiPM is nearly linear.

The SiPM simulation was constructed to supplement the other analyses and illustrate different features of the SiPM in an intuitive manner. When the results

of the simulation were compared to results from other analyses, however, it showed that there were still some flaws in the construction of the simulation. The two main things I studied in my work were SiPM nonlinearity and the pulse shape. The pulse shape from the simulation was similar to the pulse shape from test beam data, but the simulation pulse shape had a narrower base. The nonlinearity correction curve from the simulation was much lower than other experimental measurements.

The reason for the discrepancy between the simulation and other data is still being explored. There are many possibilities being considered such as the changing recharge rate of the pixel and other QIE effects. However, these effects are less understood and are harder to implement in the simulation. Once these flaws are corrected, the SiPM simulation will be a more useful tool beyond this analysis.

Because the tests on the new readout modules showed they functioned as expect, they were installed in the HE on the CMS detector during the winter of 2018. Similar readout modules, also containing SiPMs, are being constructed for the HB. While the test beam did answer many questions about the SiPM there are still features, such as nonlinearity, that could be further explored. Overall the tests and analyses on the new readout modules were very successful, and the information obtained will be used to examine the data from the CMS detector.

BIBLIOGRAPHY

[1] S. Chatrchyan *et al.*, "Observation of a new boson at a mass of 125 GeV with the CMS experiment at the LHC," *Phys. Lett.*, vol. B716, pp. 30–61, 2012.

[2] https://www.baylor.edu/physics/index.php?id=68534.

[3] S. R. Davis, "Interactive Slice of the CMS detector," Aug 2016.

[4] C. Patrignani *et al.*, "Review of Particle Physics," *Chin. Phys.*, vol. C40, no. 10, p. 100001, 2016.

[5] S. Chatrchyan *et al.*, "The CMS experiment at the CERN LHC," *JINST*, vol. 3, p. S08004, 2008.

[6] P. Cushman, A. Heering, and A. Ronzhin, "Custom HPD readout for the CMS HCAL," *Nucl. Instrum. Meth.*, vol. A442, p. 289, 2000.

[7] J. Mans, J. Anderson, B. Dahmes, P. de Barbaro, J. Freeman, T. Grassi, E. Hazen, J. Mans, R. Ruchti, I. Schimdt, T. Shaw, C. Tully, J. Whitmore, and T. Yetkin, "CMS Technical Design Report for the Phase 1 Upgrade of the Hadron Calorimeter," Tech. Rep. CERN-LHCC-2012-015. CMS-TDR-10, Sep 2012. Additional contact persons: Jeffrey Spalding, Fermilab, spalding@cern.ch, Didier Contardo, Universite Claude Bernard-Lyon I, contardo@cern.ch.

[8] S. Abdullin *et al.*, "Design, performance, and calibration of cms hadron-barrel calorimeter wedges," *Eur. Phys. J.*, vol. C55, p. 159, 2008.

[9] S. Abdullin *et al.*, "Design, performance and calibration of the CMS forward calorimeter wedges," *Eur. Phys. J.*, vol. C53, p. 139, 2008.

[10] T. Zimmerman and J.R. Hoff, "The design of a charge-integrating modified floating-point adc chip," *IEEE Journal of Solid-State Circuits*, vol. 39, p. 895, 2004.

[11] T. Shaw, A. Baumbaugh, A. Boubekeur, J. Elias, J. Hoff, S. Holm, S. Los, C. Rivetta, A. Ronzhin, J. Whitmore, T. Zimmerman, and R. Yarema, "Front end readout electronics for the cms hadron calorimeter," in *Nuclear Science Symposium Conference Record, 2002 IEEE*, vol. 1, p. 194, 2002.

[12] V. V. Abramov *et al.*, "Studies of the response of the prototype CMS hadron calorimeter, including magnetic field effects, to pion, electron, and muon beams," *Nucl. Instrum. Meth.*, vol. A457, p. 75, 2001.

[13] S. Abdullin *et al.*, "The CMS barrel calorimeter response to particle beams from 2 to 350 GeV/*c*," *Eur. Phys. J.*, vol. C60, p. 359, 2009.

[14] `https://github.com/potarf/crosstalk/tree/updates_lawrence`.